Late Cretaceous-Tertiary tectonics of the southwest Pacific: Insights from U-Pb sensitive, high-resolution ion microprobe (SHRIMP) dating of eclogite facies rocks from New Caledonia

Carl Spandler and Daniela Rubatto[1]

Department of Earth and Marine Sciences, Australian National University, Canberra, Australia

Jörg Hermann

Research School of Earth Sciences, Australian National University, Canberra, Australia

Received 6 July 2004; revised 11 January 2005; accepted 4 February 2005; published 13 May 2005.

[1] We present new U-Pb sensitive, high-resolution ion microprobe (SHRIMP) dates for zircon from eclogite facies samples from northern New Caledonia, which have important consequences for the Late Cretaceous to Eocene tectonic evolution of the southwest Pacific region. Two high-pressure metapelites contain zoned zircon crystals. Cores of these crystals represent inherited magmatic zircon grains, which yield an age of 85 Ma in both samples. Igneous zircon domains from a metamorphosed mafic cumulate and a felsic metasedimentary rock were also dated at 55 Ma. The igneous zircon of uniform age in rocks of sedimentary origin indicates that sedimentation took place from a restricted source area soon after magmatism. Therefore the protoliths of the eclogite facies rocks are considered to have formed between 85 and 55 Ma in a back-arc basin. This time period matches the age of the unmetamorphosed Poya Terrane of western New Caledonia and provides further evidence for a direct link between the two terranes. In the metapelites, irregular zircon rims that cross cut the oscillatory zoning of the cores have low trace element and Th/U contents and contain inclusions of high-pressure minerals providing evidence that these zircon rims formed during eclogite facies metamorphism. Therefore the 44.1 ± 0.9 Ma and 44.5 ± 1.2 Ma ages obtained from these rims represent burial related to subduction of the back-arc basin. It is suggested that subduction initiated soon after deposition of the youngest sediments at 55 Ma and stopped at 44 Ma during attempted subduction of continental crust, now represented as the Norfolk Ridge. Therefore the subduction system that produced the high-pressure rocks could only have operated for a maximum of 11 m.y. and would have been relatively hot. The 44 Ma age constraint for peak metamorphism also significantly predates (by 10 m.y.) the timing of obduction of the New Caledonia Ultramafic Nappe, discounting any link between obduction and high-pressure metamorphism. Combining our results with previously documented geological data, we present a revised model for the geological development of New Caledonia, which involves multiple episodes of compression and extension during the Eocene.
Citation: Spandler, C., D. Rubatto, and J. Hermann (2005), Late Cretaceous-Tertiary tectonics of the southwest Pacific: Insights from U-Pb sensitive, high-resolution ion microprobe (SHRIMP) dating of eclogite facies rocks from New Caledonia, *Tectonics*, *24*, TC3003, doi:10.1029/2004TC001709.

1. Introduction

[2] The southwest Pacific is one of the most tectonically complex regions on Earth. It consists of a number of submerged ridges and plateaus, active island arcs, oceanic spreading centers and back-arc basins (Figure 1a). Since Gondwana breakup, the region has undergone multiple episodes of continental rifting, ocean crust formation, hot spot magmatism, and subduction [*Yan and Kroenke*, 1993; *Hall*, 2002; *Crawford et al.*, 2003]. Nonetheless, our understanding of the tectonic history of the southwest Pacific is limited. Most ancient oceanic crust has been recycled back into the mantle through subduction zones and most of the subaerially exposed geology consists of volcanic islands built by relatively recent arc magmatism (<20 Ma). The timing of many tectonic events is based on interpretations of calculated plate rotation vectors or paleomagnetic data from remnants of ocean basins. It is not surprising therefore that models of plate tectonics for the region over the last 100 m.y. vary significantly [e.g., *Hall*, 2002; *Crawford et al.*, 2003; *Sdrolias et al.*, 2003].

[3] New Caledonia is centrally located in the southwest Pacific and represents the largest exposure of continental crust besides Australia and New Zealand. Its evolution is extricably linked to regional tectonics events. The northeastern portion of New Caledonia is composed of a blueschist to eclogite facies metamorphic belt that has the potential to provide crucial information on the tectonic

[1]Also at Research School of Earth Sciences, Australian National University, Canberra, Australia.

0278-7407/05/2004TC001709

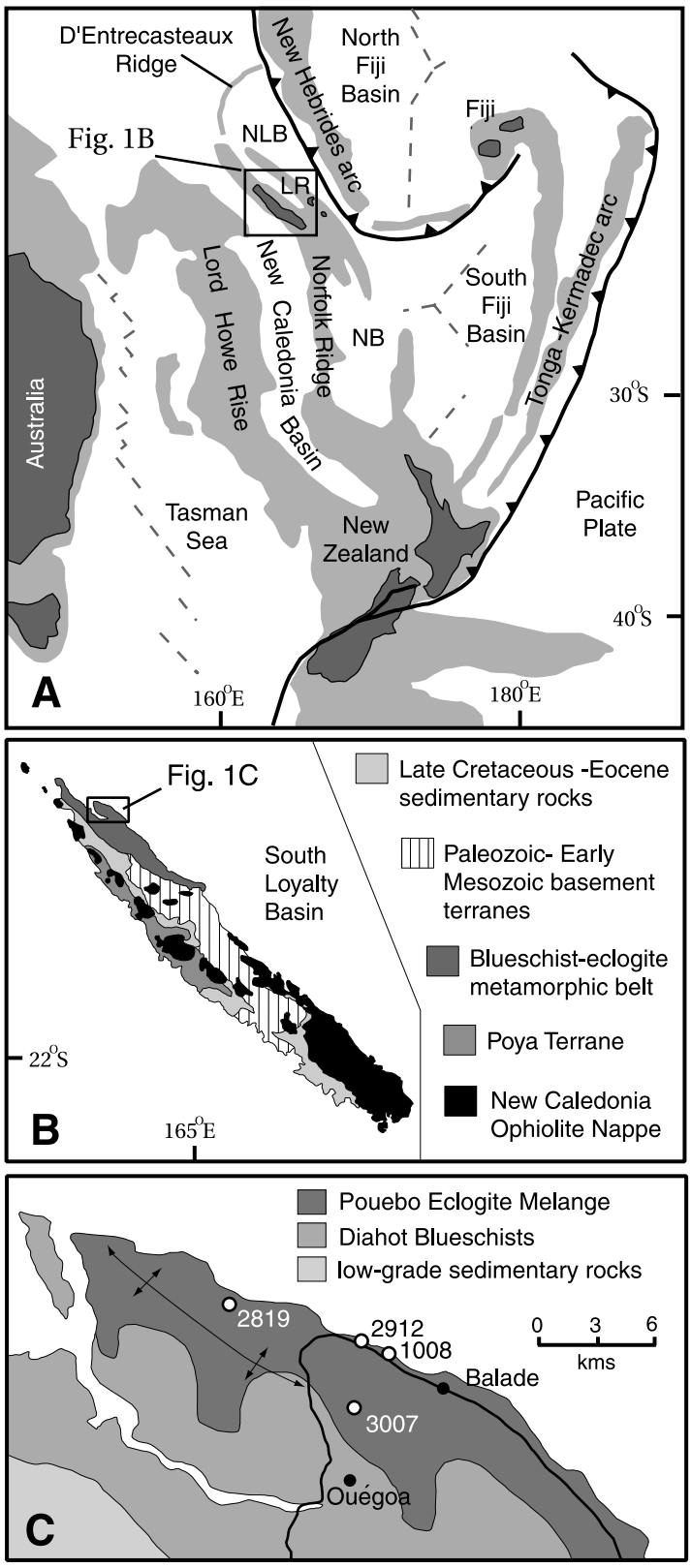

Figure 1. (a) Present-day tectonic map of the southwest Pacific. Light gray regions represent submerged continental crust and ridges. NB, Norfolk Basin; LR, Loyalty Ridge; NLB, North Loyalty Basin. (b) Major geological units of New Caledonia [after *Aitchison et al.*, 1995]. (c) Simplified geological map of the Pam Peninsula, northern New Caledonia, with sample locations.

development of the region. The high-P metamorphism and subsequent exhumation of these rocks represent major tectonic events [*Rawling and Lister*, 2002], yet there are no definitive chronological constraints on the age of the protolith rocks or the timing of metamorphism. Ion microprobe U-Pb dating has the potential to provide high-precision ages for geological events [e.g., *Williams*, 1998], yet this technique has not been widely used to constrain the timing of Late Cretaceous and Cenozoic tectonic events in the southwest Pacific.

[4] Using U-Pb sensitive, high-resolution ion microprobe (SHRIMP) geochronology, we have precisely determined the age of various generations of zircon from four eclogite facies metamorphic rocks from the belt. Combining the inclusion assemblages and geochemical characteristics for each zircon generation we have established the age of the protoliths and eclogite facies metamorphism. These results have important implications for the timing of regional geological events including ocean crust formation, sedimentation, and subduction, and allow for a greater understanding of the tectonic evolution of the southwest Pacific.

2. Geological Setting

[5] New Caledonia lies at the northern terminus of the Norfolk Ridge and is bounded by the New Caledonia Basin to the south and the North and South Loyalty Basins and Loyalty Ridge to the north (Figure 1a). The Norfolk Ridge extends southward to New Zealand and is believed to be a ribbon of Mesozoic continental crust that rifted from the Gondwana margin during the Late Cretaceous [*Sdrolias et al.*, 2003]. The Loyalty Ridge runs parallel to the Norfolk Ridge, but continues northward beyond New Caledonia as the northeast to east trending D'Entrecasteaux Ridge. The bathymetry and geochemistry of samples collected from the Loyalty-D'Entrecasteaux Ridge indicate that it is an extinct volcanic arc of Eocene age [*Eissen et al.*, 1998; *Cluzel et al.*, 2001; *Crawford et al.*, 2003]. The South Loyalty Basin extends from the Norfolk Ridge to the New Hebrides trench and underlies the Loyalty Ridge. Little is known of the origin and age of the South Loyalty Basin, although *Auzende et al.* [2000] interpreted seismic survey results to indicate a Cretaceous age of formation for the basin. The North Loyalty Basin lies between the Loyalty-D'Entrecasteaux Ridge to the south and west and the New Hebrides arc to the north. This basin is believed to have formed in a back-arc setting adjacent to the Loyalty arc [*Cluzel et al.*, 2001; *Crawford et al.*, 2003]. Stratigraphic constraints from Deep Sea Drilling Project site 286 [*Andrews et al.*, 1975] and magnetic anomaly work [*Collot et al.*, 1985; *Sdrolias et al.*, 2003] indicate that the North Loyalty Basin formed in between 56 and 35 Ma.

[6] The main island of New Caledonia consists of several mafic and ultramafic ophiolite nappes and sedimentary sequences of Cretaceous-Eocene age that have been emplaced over a series of arc-derived Mesozoic basement terranes (Figure 1b) [*Aitchison et al.*, 1995]. The extensive high-pressure (P), low-temperature (T) metamorphic belt in the northeast of the island consists of lawsonite blueschist to eclogite facies rocks [*Clarke et al.*, 1997; *Carson et al.*, 1999]. There is a rapid increase in metamorphic grade through the belt from the south and west to the northeast [*Yokoyama et al.*, 1986], which is largely due to exhumation-controlled normal faulting [*Aitchison et al.*, 1995; *Rawling and Lister*, 2002]. Protoliths of the blueschist facies rocks in the south and west of the belt are sedimentary rocks with minor intercalated basaltic to rhyolitic dikes and flows. The eclogite facies rocks of the Pam Peninsula and northeastern coastline (Figure 1c) include mafic, pelitic, and ultramafic rocks all associated as melange [*Maurizot et al.*, 1989]. In this paper these blueschist and eclogite facies units are referred to as the Diahot Blueschists and the Pouébo Eclogite Melange (PEM), respectively. Rocks of the PEM are interpreted to have a similar metamorphic history, including prograde blueschist facies metamorphism [*Clarke et al.*, 1997], followed by peak eclogite facies metamorphism ($\sim$1.9 GPa, 600°C [*Carson et al.*, 1999; *Spandler et al.*, 2003]) and finally limited greenschist facies retrogression during exhumation ($\sim$0.9 GPa, 510°C [*Marmo et al.*, 2002]). Previous cooling ages (K-Ar and ^{40}Ar-^{39}Ar) indicate that peak metamorphism occurred sometime prior to 40 Ma [*Ghent et al.*, 1994; *Baldwin et al.*, 1999]. The entire belt is interpreted to have formed during subduction of a sediment-covered back-arc basin, causing recrystallization of sedimentary and igneous protoliths under blueschist and eclogite facies conditions [*Aitchison et al.*, 1995; *Spandler et al.*, 2004a]. An extensional event following high-P metamorphism is invoked to have partly exhumed the high-P rocks [*Rawling and Lister*, 2002]. *Aitchison et al.* [1995], *Rawling and Lister* [1999], and *Fitzherbert et al.* [2004] suggested that there may be a direct link between the high-P metamorphism and the emplacement of the New Caledonia Ultramafic Nappe but up till now there is no conclusive evidence to support this link.

[7] An extensive sequence of Late Cretaceous to Eocene sandstones, siltstones, and carbonates unconformably overlie the basement terranes but is in gradational contact with the Diahot Blueschists [*Cluzel et al.*, 2001]. The lower section of the sedimentary sequence formed from volcanogenic and terrestrial material during the rifting and initial migration of New Caledonia from the Gondwana margin in the Late Cretaceous [*Aitchison et al.*, 1995, 1998]. This sequence is overlain by Paleocene to Eocene marine sediments that were deposited during postrift subsidence of New Caledonia [*Aitchison et al.*, 1995].

[8] Most of the western side of New Caledonia and several isolated exposures along the east coast are composed of a mafic rock sequence known as the Poya Terrane (Figure 1) [*Cluzel et al.*, 2001; *Eissen et al.*, 1998]. The Poya Terrane consists of pillowed and massive basalts, dolerites, and gabbros with associated cherts and volcaniclastic rocks [*Eissen et al.*, 1998] that have only been affected by sporadic low-grade metamorphism related to seafloor hydrothermal alteration [*Cluzel et al.*, 2001]. The age of the terrane is constrained by paleontological data to between 83 and 55 Ma [*Cluzel et al.*, 2001]. Geochemical [*Eissen et al.*, 1998; *Cluzel et al.*, 2001] and paleomagnetic [*Ali and Aitchison*, 2002] characteristics suggest that the

Table 1. Selected Analyses of Minerals in the Groundmass and Mineral Inclusions in Zircon Rims of Samples 1008 and 2819[a]

	Sample					
	1008				2819	
	gmass hbl	zrim hbl	gmass phg	zrim phg	gmass phg	zrim phg
SiO_2	46.18	47.60	48.23	48.89	50.04	48.83
TiO_2	0.50	0.29	0.9	0.66	0.36	0.59
Al_2O_3	12.24	10.96	27.3	27.56	27.02	27.01
Fe_2O_3	3.47	2.08				
FeO	10.61	11.85	3.41	2.56	2.13	1.81
MnO	bdl	0.12	bdl	bdl	0.07	0.17
MgO	11.46	10.79	3.12	2.67	3.57	3.14
CaO	9.31	8.25	bdl	bdl	bdl	bdl
Na_2O	3.56	3.97	0.75	0.77	0.79	0.88
K_2O	0.60	0.39	9.94	10.24	10.42	9.69
H_2O	2.05	2.03	4.38	4.39	4.44	4.35
Sum	99.98	98.33	98.03	97.74	98.84	96.47
	Molecular Formula					
O	23	23	22	22	22	22
Si	6.70	7.00	6.61	6.69	6.76	6.73
Ti	0.05	0.03	0.09	0.07	0.04	0.06
Al	2.09	1.90	4.41	4.44	4.30	4.39
Fe^{3+}	0.38	0.23				
Fe^{2+}	1.29	1.46	0.39	0.29	0.24	0.21
Mn	-	0.01	-	-	0.01	0.02
Mg	2.48	2.37	0.64	0.54	0.72	0.64
Ca	1.45	1.30	-	-	-	-
Na	1.00	1.13	0.20	0.20	0.21	0.24
K	0.11	0.07	1.74	1.79	1.79	1.7
Cation sum	15.55	15.50	14.08	14.02	14.07	13.99

[a]The molecular formula for hornblende was calculating assuming $\sum$(cations -Na-Ca-K) = 13. Fe^{2+} and Fe^{3+} for hornblende were calculated on the basis of charge balance. All Fe was assumed to be Fe^{2+} for phengite. H_2O was calculated assuming stoichiometric mineral compositions. The low totals for the inclusion analyses are due to undercutting of inclusions during sample polishing and interference from the zircon host. Host are gmass, groundmass; zrim, zircon rims; minerals are bdl, below detection limit; hbl, hornblende; phg, phengite.

terrane formed as oceanic crust in a back-arc basin to the northeast of New Caledonia and was thrust over the island in the mid-Eocene. Geochemical comparisons between mafic rocks from the Poya Terrane and the PEM indicate that the two geological units are genetically related [*Cluzel et al.*, 2001; *Spandler et al.*, 2004a].

[9] The final major tectonic event to affect New Caledonia was the obduction of the New Caledonia Ultramafic Nappe over the island at approximately 34 Ma [*Cluzel et al.*, 2001]. The Ultramafic Nappe currently covers over a third of the island and largely consists of dunite and harzburgite, although gabbroic rocks of the upper parts of the sequence are still preserved in some places. The Ultramafic Nappe is continuous with basement rocks of the South Loyalty Basin and is interpreted to have formed as part of a forearc mantle lithosphere to the north of the New Caledonia [*Collot et al.*, 1987; *Aitchison et al.*, 1995; *Auzende et al.*, 2000]. Mafic dikes with suprasubduction zone (SSZ) geochemical signatures cut the ultramafic rocks and have been dated to ~50 Ma [*Cluzel et al.*, 2001]. Unaltered boninites of expected late Paleocene-Eocene age are also associated with the ultramafic nappe in a number of localities [*Eissen et al.*, 1998].

3. Analytical Techniques

3.1. Mineral Compositions

[10] Major element compositions for minerals and mineral inclusions in zircon were determined using an energy-dispersive spectrometer equipped, JEOL 6400 scanning electron microscope (SEM), at the Electron Microscope Unit, Australian National University (ANU). Accelerating voltage, beam current and counting time were set at 15 kV, 1 nA, and 100 s, respectively. Many of the mineral inclusions are too small (<3 μm) to avoid minor interference from the zircon host and hence major element totals are often a few percent lower that the expected totals (Table 1).

3.2. Zircon and Bulk Rock Geochemistry

[11] Trace element concentrations in zircon were acquired by laser ablation, inductively coupled-plasma mass spectrometry (LA ICP-MS) at the Research School of Earth Sciences (RSES), ANU. The LA ICP-MS employs an ArF (193 nm) EXCIMER laser and a Hewlett Packard Agilent 7500 ICP-MS. Laser sampling was performed in an Ar-He atmosphere using a spot size between 19 and 40 μm. The counting time was 20 s for the background and 60–80 s for sample analysis, and instrument calibration was against NIST 612 glass using standard reference values of *Pearce et al.* [1997]. Silicon was used as an internal standard assuming ideal zircon stoichiometry (SiO_2 = 32.45 wt %). During the time-resolved analysis, contamination from inclusions and fractures and zones of different composition were detected by monitoring several elements. Analyses with excessive interference from inclusions were not used. Whole rock major and trace element concentrations were determined on Li-Borate glass discs fused with rock powder by XRF spectrometry and LA ICP-MS, respectively. Details of these analytical procedures are given by *Spandler et al.* [2003].

3.3. U-Pb Geochronology

[12] Zircon was prepared as mineral separates mounted in epoxy and polished down to expose the grain centers. Cathodoluminescence imaging was carried out at the Electron Microscope Unit, ANU, with a HITACHI S2250-N SEM operating at 15 kV, ~60 μA, and ~20 mm working distance. U-Th-Pb analyses were performed using the sensitive, high-resolution ion microprobes (SHRIMP II and reverse geometry (RG)) at the RSES, ANU. Instrumental conditions and data acquisition were generally as described by *Compston et al.* [1992] and *Williams* [1998]. The data were collected in sets of seven scans throughout the masses. The measured $^{206}Pb/^{238}U$ ratio was corrected using reference zircon TEM from the Middledale gabbroic diorite [*Black et al.*, 2003], whereas a zircon of known composition (SL 13) was used to determine the U content of the target. The analyses were corrected for common Pb on the basis of the measured $^{207}Pb/^{206}Pb$ as described by *Compston et al.*

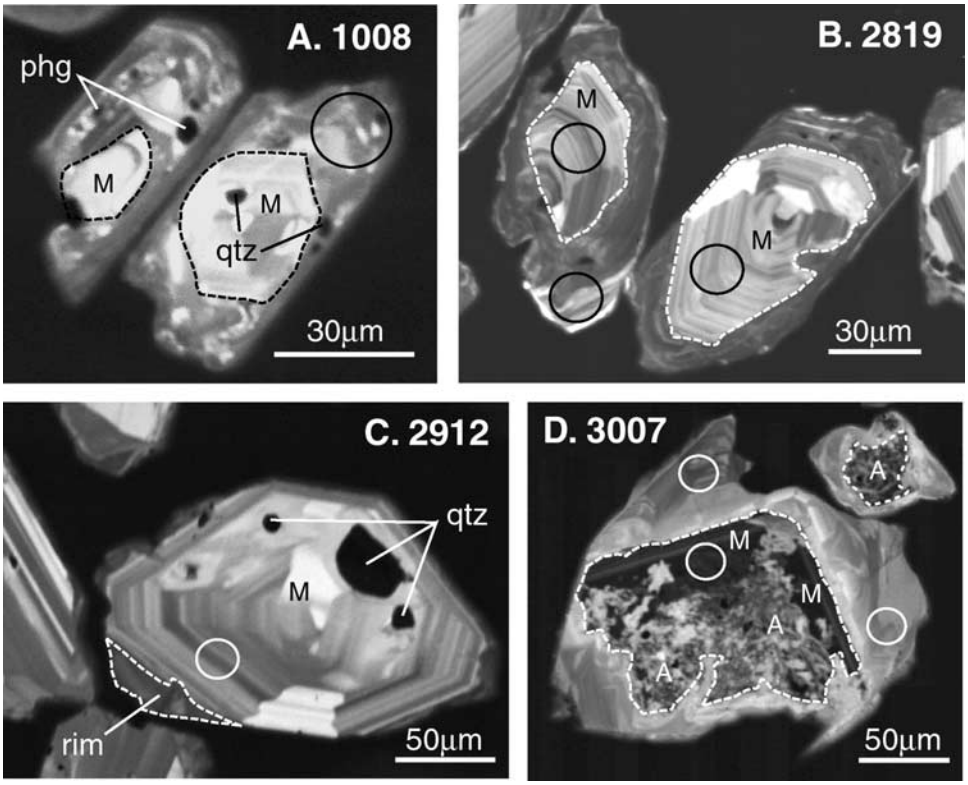

Figure 2. Cathodoluminescence (CL) images of zircon crystals from samples (a) 1008, (b) 2819, (c) 2912, and (d) 3007. Circles indicate the location of SHRIMP analyses. The dotted lines are used to delineate core and rim domains. M, magmatic core domain; A, altered core domain; phg, phengite; qtz, quartz. Additional CL images of zircon grains from sample 3007 are presented by *Spandler et al.* [2004b].

[1992]. Owing to the young age and the low U content of the samples, some analyses have a high proportion of common Pb. However, in absolute amount, the common Pb content of the samples is similar to that of the common Pb free standard. This indicates that the common Pb is mainly surface and instrumental background, the composition of which is known to be that of Broken Hill Pb ($^{204}Pb/^{206}Pb$ = 0.0625, $^{207}Pb/^{206}Pb$ = 0.9618, $^{208}Pb/^{206}Pb$ = 2.2285). None of the calculated mean ages would change significantly if a different common Pb composition is used. Age calculations were conducted by regressing uncorrected analysis to the Broken Hill common Pb composition in a Tera-Wasserburg diagram using the software Isoplot/Ex [*Ludwig*, 2000]. Isotopic ratios and single ages are reported with 1sigma errors, whereas mean ages are at 95% confidence level.

4. Sample Description

4.1. Samples 1008 and 2819

[13] Samples 1008 and 2819 are coarse-grained, foliated pelitic schists that occur in the PEM along the eastern coast of the Pam Peninsula where the highest-grade rocks crop out (Figure 1c). The samples largely consist of quartz, phengite, and garnet and have epidote, allanite, apatite, rutile, and zircon as accessory minerals. Barroisitic hornblende and chlorite are minor phases in 1008 and 2819, respectively. The typical eclogite facies paragenesis of garnet+omphacite occurs in associated eclogites [*Clarke et al.*, 1997], providing evidence that the whole rock suite experienced eclogite facies metamorphism. Na-rich mafic rocks and the pelitic rocks are omphacite free due to their bulk rock composition. However, the mineral assemblages of the investigated metapelites are clearly distinct from assemblages of metapelites from the lawsonite blueschist zone [*Yokoyama et al.*, 1986]. On the basis of mineral compositions and calculated metamorphic temperatures it has been suggested that these metapelites record the same peak metamorphic conditions as the associated eclogites [*Spandler et al.*, 2003]. Evidence of retrogression is absent in 2819 and only manifests as thin glaucophane rims on hornblende in sample 1008. A more detailed mineralogical and geochemical description of sample 1008 has been presented previously by *Spandler et al.* [2003].

[14] Zircon grains from sample 1008 generally are euhedral, elongated, clear, and rarely excess 100 μm in size. In sample 2819, the zircon crystals are more variable in size (30–250 μm), but tend to be prismatic and euhedral in shape, and may be either clear and colorless or pale yellow. In CL (Figure 2) zircon grains from both samples have similar features; a highly luminescent core, irregular in

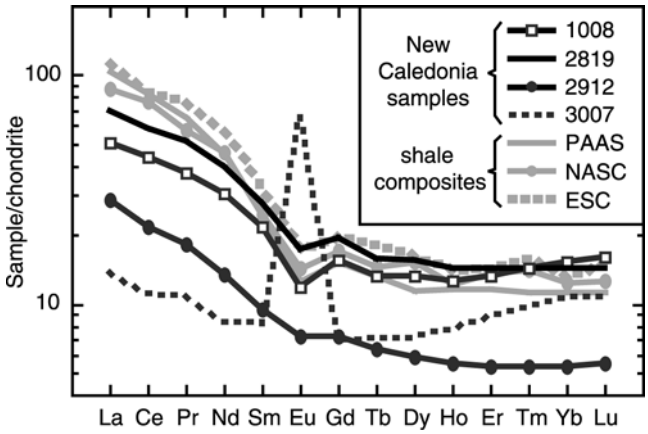

Figure 3. Chondrite-normalized rare earth element patterns for eclogite facies samples from New Caledonia. Also shown are patterns for post-Archean Australian shale (PAAS), North American shale composite (NASC), and European shale composite (ESC). Values for chondrite and shale composites are from *Taylor and McLennan* [1985].

shape, surrounded by a darker rim less than 50 μm in width. The cores usually feature fine oscillatory or sector zoning, which is truncated by the rim. The rims lack any regular zoning patterns, although faint irregular and discontinuous banding is preserved in places. Mineral inclusion assemblages in zircon are also similar in both samples. The cores have relatively rare inclusions of apatite and quartz, whereas the rims have abundant inclusions of quartz, phengite, apatite, barroisitic hornblende, allanite, and epidote in sample 1008 and quartz, phengite, epidote, and paragonite in sample 2819. The compositions of the mineral inclusions in the zircon rims are indistinguishable from the compositions of groundmass minerals in most cases (Table 1).

4.2. Sample 2912

[15] Sample 2912 was also collected from an outcrop along the eastern coast of the Pam Peninsula (Figure 1c). The outcrop consists of coarse, unfoliated felsic rock that has distinct banding defined by glaucophane-bearing and glaucophane-absent zones. 2912 is a sample of a glaucophane-bearing horizon and largely consists of quartz, coarse phengite, porphyroblastic garnet, and tabular epidote. Glaucophane and paragonite are minor constituents and rutile, allanite, and zircon occur in trace amounts. Minor retrogression is evident from partial replacement of garnet and glaucophane by chlorite. The quartz content is significantly higher in sample 2912 than in samples 1008 or 2819.

[16] Zircon grains are clear, colorless, idiomorphic and may reach 300 μm in size. Almost all zircon grains have well-developed oscillatory or sector zoning that are clearly distinguishable in CL images. Thin (<10 μm) low CL intensity rims are occasionally present (Figure 2c). Apatite, quartz, paragonite, and phengite have been identified as inclusions in zircon, but the inclusions of paragonite and phengite either lie along cracks in the zircon or are associated with the thin zircon rim overgrowths. Only apatite and quartz can be directly associated with crystallization of the zircon cores.

4.3. Sample 3007

[17] Sample 3007 was collected from a ridgeline outcrop north of Ouégoa (Figure 1c) in an area consisting of eclogites, garnet blueschists, pelitic schists, and serpentinites. 3007 is a sample of a discordant zone in a high-P mafic-felsic layered sequence. The sample consists almost completely of coarse phengite, chlorite, epidote, and tremolite, though apatite and zircon are rare accessory phases. Zircon grains are variable in size (50 to 300 μm) and transparent to pale brown in color. Three distinct zircon types were identified using CL imaging (Figure 2d). The most pristine sections of the zircon cores have euhedral to subhedral forms, low CL intensities and mild oscillatory zoning. Mineral inclusions were not identified in this zircon type. However, most of the zircon cores have experienced recrystallization, producing zircon domains that have chaotic internal zoning features and abundant mineral inclusions (kaolinite, celadonite, quartz, Fe oxy-hydroxide, chlorite-smectite mixtures, thortveitite ($Sc_2Si_2O_7$), yttrialite ($Y_2Si_2O_7$), xenotime, and allanite). A detailed discussion of this mineral assemblage is presented by *Spandler et al.* [2004b]. Most zircon grains have distinct rims that have intermediate CL intensities and rounded to irregular outer morphologies. Wavy, discontinuous and convoluted banding and fine-scale oscillatory zoning is common in these rims and in some grains the rim domain embays the altered cores (Figure 2) [*Spandler et al.*, 2004b]. It is clear that the rims surround and crosscut textural features of the cores, indicating that the alteration of the cores predates the formation of the zircon rims. The zircon rims contain rare inclusions of relatively high-Ti phengite, epidote, barroisitic hornblende, and talc.

5. Bulk Rock and Zircon Geochemistry

[18] The major and trace element chemical composition of all four samples was determined to aid in establishing the nature and origin of the protoliths. These data are available as auxiliary material[1]. Pelitic samples 2819 and 1008 are remarkably similar in composition and closely compare to various average shale composites (Figure 3) and average subducting sediment [*Spandler et al.*, 2003]. An igneous origin for these samples is discounted based on the high Mg and Fe for the given Si and K content. Sample 2912 is also felsic in composition but has higher Si, Ca, and Al, and lower Fe, Mg, and most trace elements than samples 1008 and 2819. Sample 2912 has a major element composition that is similar to granitic or rhyolitic rocks, but the rare earth element pattern only features a very slight negative Eu anomaly, which is uncharacteristic of highly differentiated igneous rocks [*Taylor and McLennan*, 1985]. The geochemistry and origin of sample 3007 has been discussed in detail by *Spandler et al.* [2004b]. The rock is mafic in composition with high concentrations of Al, Sr, U, and large-ion

[1] Auxiliary material is available at ftp://ftp.agu.org/apend/tc/2004TC001709.

lithophile elements. The rare earth element (REE) pattern features a large positive Eu anomaly (Figure 3). On the basis of these features and the assemblage of mineral inclusions in zircon, the protolith for the sample is suggested to be a hydrothermally altered, plagioclase-rich mafic cumulate [*Spandler et al.*, 2004b].

[19] Trace element data from zircon is presented in Table 2, Figure 4, and the auxiliary material. Zircon cores from sample 2819 have medium to high Th (63–948 ppm) and U (85–697 ppm) contents resulting in Th/U of 0.6–1.5. The chondrite-normalized REE patterns feature a strong heavy REE (HREE) enrichment (Lu_N/Gd_N = 11–44), and marked positive Ce anomaly and negative Eu anomaly (Eu/Eu* = 0.18–0.35). The rims have significantly lower Th, U, and other trace element contents. The Th/U is as low as 0.007 and the REE patterns lack distinct Ce and Eu anomalies (Eu/Eu* $\sim$ 0.5–0.6). Zircon crystals from sample 1008 have not been analyzed for trace elements by LA ICP-MS, but cores and rims have similar U, Th, and Th/U (0.55–1.56 cores; 0.002–0.11 rims) to the respective zircon domains in sample 2819.

[20] Zircon from sample 2912 has medium to low U (22–109 ppm) and Th (12–45 ppm) contents with rather constant Th/U around 0.3. REE patterns are similar to those of zircon cores in 2819, except that light REE (LREE) contents are lower and the negative Eu anomaly is slightly less pronounced (Eu/Eu* = 0.26–0.46). This feature is also present in the bulk-rock, suggesting that the zircon is reflecting the bulk rock composition.

[21] The pristine zircon cores in sample 3007 also have igneous characteristics including high Nb, Th, U, Th/U (0.14–2.1), and REE patterns with HREE enrichment, a positive Ce anomaly and a strong negative Eu anomaly (Eu/Eu* = 0.024–0.35). In this case the Eu anomaly is clearly related to magmatic processes. The bulk rock composition displays a large positive Eu and Sr anomaly indicative of extensive plagioclase crystallization [*Spandler et al.*, 2004b]. Zircon most likely formed from a residual melt which was enriched in REE but depleted in Eu due to previous plagioclase crystallization. As with sample 2819, the zircon rims in 3007 are depleted in trace elements with respect to the magmatic cores and generally have low Th/U. The REE patterns are relatively enriched in HREE and have no apparent Ce or Eu anomalies.

6. U-Pb Geochronology

6.1. SHRIMP Results

[22] Isotopic analyses on zircon from the pelitic schists 2819 and 1008 confirm the presence of two domains as indicated by CL and trace element characteristics. Ten analyses on zircon cores of sample 2819 yield $^{206}Pb/^{238}U$ ages tightly grouped around 85 Ma (Table 2). In the Tera-Wasserburg diagram (Figure 5) the 10 analyses plot on a regression line forced to Broken Hill common Pb, which intercept the Concordia at 84.8 ± 0.9 Ma (mean square weighted deviation (MSWD) = 1.3). One single core analysis yielded a significantly younger age of 77.7 ± 1.7 Ma, probably because of overlap with the rim as indicated by low Th and U contents. The rims yield $^{206}Pb/^{238}U$ ages between 39.9 ± 1.1 and 46.3 ± 1.5 Ma. Statistical treatment indicated that three analyses are younger than the main group and these were excluded from the age calculation due to suspected Pb loss. The remaining ten analyses were regressed to common Pb on a Tera-Wasserburg diagram and define an age of 44.1 ± 0.9 Ma (MSWD = 1.12).

[23] Five analyses on zircon cores from sample 1008 define an average age of 84.9 ± 4.3 Ma (MSWD = 2.9). One small core produced a younger age, as the analysis probably partly overlapped with the zircon rim. The low Th/U rims consistently yielded middle Eocene ages. The regression to common Pb in the Tera-Wasserburg diagram gives an average age of 44.5 ± 1.2 Ma (MSWD = 3.0). Two analyses on rims are significantly older, most likely due to mixed analysis with the core. The relatively high MSWD for these ages is partly due to analytical spread in the SHRIMP RG session during which sample 1008 was analyzed.

[24] Twelve analyses of the zoned zircon cores of samples 2912 form a tight cluster on the Tera-Wasserburg diagram (Figure 5) and define an age of 55.3 ± 0.8 Ma (MSWD = 0.7). The zircon rim domains in this sample could not be dated due to their small size.

[25] Of the three zircon domains identified in sample 3007 with CL and discussed in detail by *Spandler et al.* [2004b], effort was only made to date the pristine cores and the rims by SHRIMP. The zircon cores, which are rich in U and Th, yielded late Paleocene–early Eocene ages around 55 Ma. With the exclusion of one significantly younger analysis (3007–15.1), the data lay on a regression line to common Pb that defines an average age of 55.6 ± 0.5 Ma (MSWD = 1.04). The rims have extremely low U contents (1–20 ppm) and thus low radiogenic Pb. Therefore, in many of the analyses the amount of common Pb is more than 50% of the measured Pb. Accurate age calculations from these analyses were not possible, so these data were discarded and are not presented in Table 2. The remaining 10 analyses of zircon rims have variable Th/U, because of the large uncertainty related to the measurement of such small concentrations. The single spot ages scatter between 24.6 ± 5.1 and 52.1 ± 2.6 Ma and have relatively large errors because of the low isotopic concentrations. The three youngest rims are outliers of a main group that on the Tera-Wasserburg diagram defines an age of 47.9 ± 5.3 Ma (MSWD = 5.2). Despite the dispersion of ages indicated by the large MSWD, this is the best estimate of the age of the rims. Only one analysis was taken on the altered zircon domains, which yielded an age of 46.1 ± 1.3 Ma and an unusually high Th/U of 2.15. These domains have undergone hydrothermal alteration [*Spandler et al.*, 2004b] that is expected to have disturbed the U-Th-Pb systematics. In fact, isotopic analyses from zircon with similar features are generally discordant and geologically meaningless [e.g., *Tomaschek et al.*, 2003; D. Rubatto, unpublished data, 2003]. For these reasons no further attempt was made to date the altered cores.

6.2. Age Interpretations

[26] U-Pb dating of the selected samples falls in three age groups of circa 85, 55, and 44 Ma, (Figure 6) the interpre-

Table 2. U-Th-Pb SHRIMP Zircon Data

Label	Zircon domain	U (ppm)	Th(ppm)	Th/U	% ^{204}Pb	^{238}U/^{206}Pb ± 1s	^{207}Pb/^{206}Pb ± 1s	Age ± 1s (Ma)
				Pelitic Schist Sample 2819				
7.1	rim	116	14	0.12	11.45	126.82 ± 5.35	0.1375 ± 0.0127	45.6 ± 2.1
8.1	rim	34	1.8	0.053	19.88	125.73 ± 7.58	0.2042 ± 0.0282	42.3 ± 3.1
9.1	rim	25	0.28	0.011	23.72	120.82 ± 4.30	0.2346 ± 0.0166	42.3 ± 2.1
10.1[a]	rim	203	1.5	0.007	4.69	156.51 ± 3.11	0.0839 ± 0.0052	39.4 ± 0.8
11.1	rim	92	1.9	0.021	16.87	131.32 ± 4.27	0.1804 ± 0.0071	41.8 ± 1.6
13.1[a]	rim	78	0.14	0.002	2.28	170.76 ± 4.08	0.0648 ± 0.0068	36.8 ± 0.9
5.2	rim	64	1.5	0.024	7.43	129.86 ± 3.77	0.1058 ± 0.0098	46.3 ± 1.5
14.1[a]	rim	57	0.35	0.006	4.65	154.65 ± 4.19	0.0836 ± 0.0081	39.9 ± 1.1
15.1	rim	115	1.7	0.015	11.18	132.99 ± 2.72	0.1354 ± 0.0094	43.6 ± 1.1
16.1	rim	43	0.35	0.008	11.90	125.69 ± 4.03	0.1411 ± 0.0125	45.8 ± 1.7
17.1	rim	35	1.7	0.048	13.50	125.39 ± 3.85	0.1538 ± 0.0106	45.2 ± 1.6
18.1	rim	64	0.80	0.013	4.75	143.39 ± 3.61	0.0845 ± 0.0057	43.0 ± 1.1
25.1	rim	37	0.93	0.025	8.61	132.49 ± 4.51	0.1150 ± 0.0112	44.9 ± 1.7
9.2[a]	mixed	121	72	0.60	2.40	80.77 ± 1.71	0.0666 ± 0.0072	77.7 ± 1.7
19.1c	core	206	125	0.61	0.18	74.91 ± 1.26	0.0491 ± 0.0018	85.4 ± 1.4
20.1c	core	200	181	0.91	0.36	76.55 ± 1.45	0.0505 ± 0.0020	83.4 ± 1.5
21.1c	core	178	210	1.18	0.25	76.51 ± 1.30	0.0497 ± 0.0019	84.6 ± 1.4
13.2c	core	269	250	0.93	0.85	76.15 ± 1.25	0.0544 ± 0.0017	83.5 ± 1.3
14.2c	core	126	128	1.02	0.96	75.83 ± 1.40	0.0553 ± 0.0030	83.8 ± 1.5
22.1c	core	380	376	0.99	0.15	73.72 ± 1.15	0.0489 ± 0.0013	86.7 ± 1.3
17.2c	core	258	241	0.93	0.63	76.62 ± 1.32	0.0527 ± 0.0018	83.1 ± 1.4
23.1c	core	509	700	1.38	0.31	72.74 ± 1.19	0.0502 ± 0.0011	87.8 ± 1.4
24.1c	core	283	335	1.18	3.55	73.35 ± 1.19	0.0759 ± 0.0019	84.6 ± 1.3
25.2c	core	336	284	0.84	0.56	76.38 ± 1.21	0.0521 ± 0.0014	83.4 ± 1.2
				Pelitic Schist Sample 1008				
1.1	rim	51	0.62	0.012	18.39	111.79 ± 3.41	0.1926 ± 0.0126	48.3 ± 1.9
2.1	rim	39	0.50	0.013	4.31	130.25 ± 4.43	0.0811 ± 0.0074	47.5 ± 1.6
2.2	rim	21	0.12	0.006	11.42	130.06 ± 5.40	0.1373 ± 0.0194	44.5 ± 2.2
3.1	rim	44	0.18	0.004	4.40	127.96 ± 4.18	0.0818 ± 0.0068	48.3 ± 1.6
4.1	rim	43	0.22	0.005	7.23	149.03 ± 5.11	0.1041 ± 0.0090	40.4 ± 1.4
5.1	rim	194	0.44	0.002	1.28	136.81 ± 3.46	0.0570 ± 0.0023	46.4 ± 1.1
6.1	rim	46	0.14	0.003	3.91	153.69 ± 5.28	0.0777 ± 0.0061	40.4 ± 1.4
7.1	rim	47	5.1	0.11	4.31	147.28 ± 5.20	0.0809 ± 0.0064	42.0 ± 1.5
7.2	rim	81	5.4	0.067	3.99	164.62 ± 4.78	0.0784 ± 0.0054	40.1 ± 1.2
10.1	rim	147	0.46	0.003	0.48	138.97 ± 3.68	0.0507 ± 0.0031	46.0 ± 1.2
11.1	rim	90	3.1	0.034	19.27	116.31 ± 3.32	0.1995 ± 0.0115	46.0 ± 1.8
12.1	rim	131	1.0	0.008	1.73	140.17 ± 3.82	0.0606 ± 0.0048	45.1 ± 1.2
13.1	rim	44	0.07	0.002	6.44	143.55 ± 5.12	0.0978 ± 0.0074	42.3 ± 1.5
14.1	rim	111	0.62	0.006	2.22	141.32 ± 4.01	0.0645 ± 0.0036	44.6 ± 1.2
15.1	rim	84	0.33	0.004	1.96	140.55 ± 4.07	0.0624 ± 0.0038	44.9 ± 1.3
16.1	rim	33	0.39	0.012	9.29	138.28 ± 5.16	0.1204 ± 0.0100	42.7 ± 1.7
17.1	rim	104	0.23	0.002	2.57	144.32 ± 4.07	0.0672 ± 0.0037	43.5 ± 1.2
11.2	rim	19	0.89	0.047	13.12	138.93 ± 8.69	0.1506 ± 0.0137	41.0 ± 2.7
20.1	rim	17	0.39	0.023	13.15	132.09 ± 6.03	0.1509 ± 0.0132	43.1 ± 2.1
18.1[a]	mixed	104	44	0.42	1.09	107.13 ± 2.82	0.0558 ± 0.0027	59.3 ± 1.5
9.1[a]	mixed	339	180	0.53	1.40	87.31 ± 2.16	0.0586 ± 0.0023	72.5 ± 1.7
19.1[a]	mixed	321	58	0.18	4.13	125.72 ± 3.36	0.0797 ± 0.0040	49.3 ± 1.3
4.2c	core	80	84	1.04	10.06	70.39 ± 1.86	0.1275 ± 0.0060	83.1 ± 2.3
21.1c	core	598	935	1.56	0.21	73.21 ± 1.70	0.0495 ± 0.0008	87.3 ± 1.9
22.1c	core	163	132	0.81	0.51	80.47 ± 1.96	0.0516 ± 0.0018	79.3 ± 1.8
23.1c	core	199	145	0.73	0.19	73.05 ± 1.74	0.0492 ± 0.0017	87.5 ± 2.0
24.1c	core	254	139	0.55	1.40	73.73 ± 1.74	0.0588 ± 0.0015	85.8 ± 1.9
				Garnet-Quartz-Phengite Gneiss Sample 2912				
2.1c	core	95	35	0.37	8.14	113.38 ± 3.36	0.0694 ± 0.0038	55.2 ± 1.6
3.1c	core	107	45	0.42	3.47	118.71 ± 2.41	0.0535 ± 0.0035	53.7 ± 1.1
4.1c	core	87	30	0.34	11.01	112.17 ± 3.60	0.0683 ± 0.0042	55.9 ± 1.8
5.1c	core	109	25	0.23	3.75	117.06 ± 3.14	0.0589 ± 0.0033	54.1 ± 1.4
6.1c	core	79	29	0.36	0.00	114.72 ± 3.81	0.0557 ± 0.0041	55.4 ± 1.8
7.1c	core	74	35	0.47	0.00	109.14 ± 2.44	0.0639 ± 0.0040	57.7 ± 1.3
8.1c	core	98	42	0.43	0.00	112.6 ± 2.79	0.0574 ± 0.0033	56.4 ± 1.4
9.1c	core	87	27	0.31	7.11	113.05 ± 2.44	0.0673 ± 0.0043	55.5 ± 1.2
10.1c	core	58	21	0.36	0.00	112.72 ± 2.72	0.0676 ± 0.0047	55.7 ± 1.3
11.1c	core	70	20	0.29	14.35	115.93 ± 2.65	0.0597 ± 0.0041	54.6 ± 1.2
12.1c	core	106	39	0.37	5.05	115.68 ± 2.37	0.0594 ± 0.0033	54.7 ± 1.1
13.1c	core	94	37	0.39	4.64	113.28 ± 2.38	0.0667 ± 0.0045	55.4 ± 1.2

Table 2. (continued)

Label	Zircon domain	U (ppm)	Th(ppm)	Th/U	% ^{204}Pb	^{238}U/^{206}Pb ± 1s	^{207}Pb/^{206}Pb ± 1s	Age ± 1s (Ma)
Chlorite-Epidote-Phengite Schist Sample 3007								
27.1c	core	828	732	0.88	1.34	115.97 ± 1.84	0.0498 ± 0.0011	55.2 ± 0.8
10.2c	core	1063	61	0.057	0.00	114.02 ± 1.72	0.0522 ± 0.0013	56.0 ± 0.8
20.2c	core	1237	364	0.29	0.53	114.41 ± 1.71	0.0512 ± 0.0009	55.8 ± 0.8
28.1c	core	540	492	0.91	2.54	117.29 ± 1.84	0.0531 ± 0.0014	54.4 ± 0.8
29.1c	core	904	197	0.22	1.18	114.62 ± 1.86	0.0491 ± 0.0010	55.9 ± 0.9
3.2c	core	614	792	1.29	0.00	112.7 ± 1.75	0.0527 ± 0.0014	56.6 ± 0.8
6.1c	core	706	196	0.28	0.02	113.51 ± 2.04	0.0472 ± 0.0010	56.5 ± 1.0
8.2c	core	2015	2424	1.20	1.36	120.63 ± 4.22	0.0594 ± 0.0016	50.9 ± 1.2
10.1c	core	967	912	0.94	14.83	97.95 ± 1.74	0.1827 ± 0.0025	56.1 ± 1.5
15.1c[a]	core	1775	2793	1.57	0.35	127.43 ± 4.82	0.0502 ± 0.0009	52.1 ± 1.1
18.1c	core	725	600	0.83	0.04	119.01 ± 2.09	0.0474 ± 0.0013	53.5 ± 1.0
20.1c	core	1078	224	0.21	0.14	115.45 ± 1.92	0.0483 ± 0.0008	58.1 ± 1.0
22.1c	core	750	500	0.67	1.62	111.35 ± 1.94	0.0618 ± 0.0014	57.1 ± 1.0
25.1c	core	896	125	0.14	0.14	117.21 ± 2.17	0.0483 ± 0.0013	55.1 ± 1.0
1.2	altered core	230	494	2.15	1.79	137.33 ± 3.30	0.0664 ± 0.0025	46.1 ± 1.3
1.1	rim	4.6	0.01	0.002	21.8	130.95 ± 9.96	0.2562 ± 0.0407	38.1 ± 3.9
5.1	rim	3.6	4.9	1.35	49.2	60.00 ± 4.87	0.5451 ± 0.0533	49.1 ± 9.8
8.3	rim	4.6	0.004	0.001	46.9	97.37 ± 17.25	0.4452 ± 0.0527	37.5 ± 8.3
9.1	rim	5.1	0.1	0.022	18.6	101.25 ± 7.79	0.2513 ± 0.0373	49.6 ± 4.9
13.1	rim	20	7.7	0.39	17.8	100.68 ± 3.47	0.2195 ± 0.0162	52.1 ± 2.6
14.1	rim	9.1	0.2	0.017	32.6	93.22 ± 4.23	0.4075 ± 0.0313	42.0 ± 4.3
21.1	rim	2.5	1.0	0.40	32.5	84.29 ± 9.15	0.3684 ± 0.0519	49.7 ± 7.6
23.1	rim	6.9	1.3	0.20	23.5	147.91 ± 8.24	0.2605 ± 0.0305	33.5 ± 2.7
9.2	rim	3.6	0.1	0.04	26.0	134.3 ± 14.58	0.3025 ± 0.0464	34.7 ± 4.8
7.1	rim	3.6	2.5	0.70	38.7	146.36 ± 18.74	0.4519 ± 0.0698	24.6 ± 5.1

[a]Excluded from the mean age calculation mixed domain represent a mix between core and rim.

tation of which is discussed below in the light of CL, mineral inclusions, and trace element data. The Late Cretaceous age of 85 Ma was measured in zircon cores that have magmatic textural features such as oscillatory and sector zoning and preserved euhedral crystal faces [*Rubatto and Gebauer*, 2000; *Corfu et al.*, 2003]. Th-U ratio is often used to distinguish magmatic versus metamorphic zircon, and is in the range 0.5–1.6 for the 85 Ma zircon. This range is

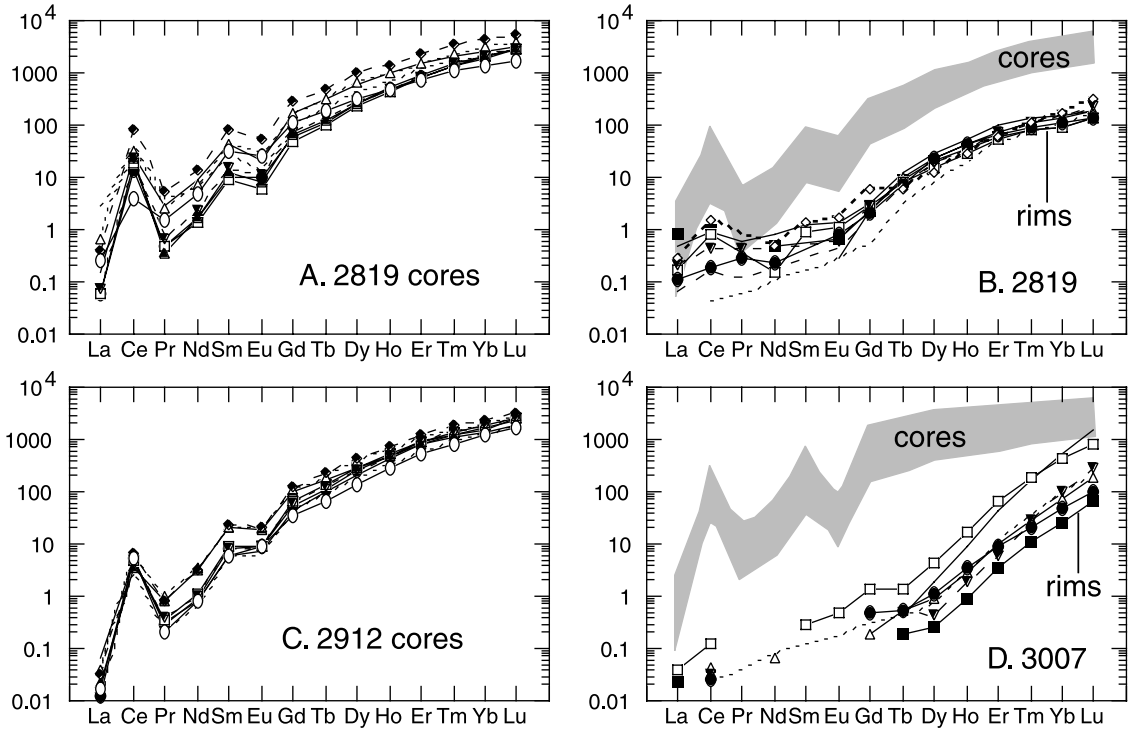

Figure 4. Chondrite-normalized rare earth element patterns for zircon crystals from samples (a, b) 2819, (c) 2912, and (d) 3007. Chondrite values are from *Taylor and McLennan* [1985].

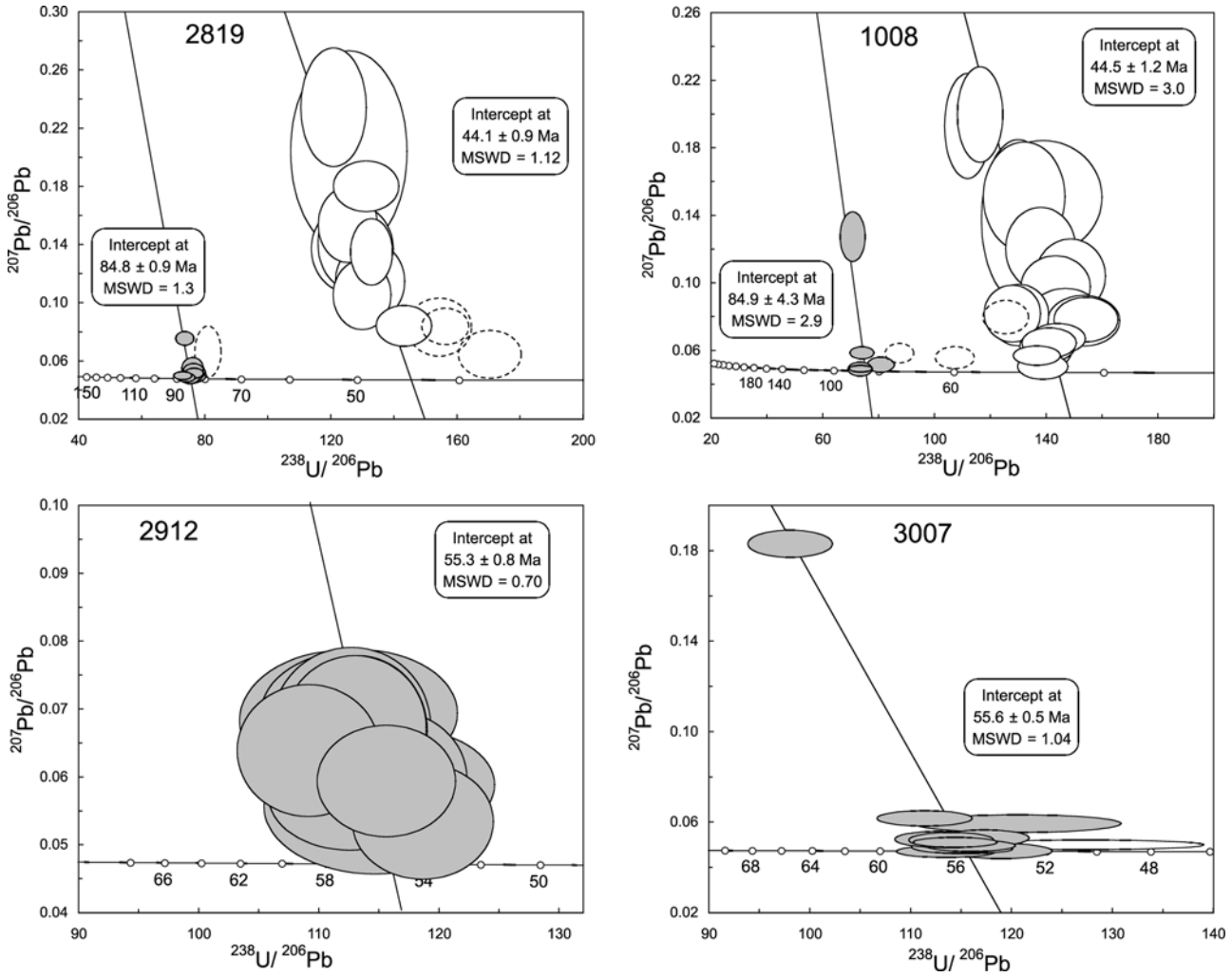

Figure 5. Tera-Wasserburg diagrams for uncorrected U-Pb data. Ages are defined by the intercept of Concordia with the regression line to common Pb. Error ellipses represent 2σ. Data plotted as dashed ellipses are excluded from the age calculations. Numbers on the Concordia lines are in millions of years.

equivalent to that documented for magmatic zircon [e.g., *Williams*, 1998; *Rubatto and Gebauer*, 2000; *Hoskin and Schaltegger*, 2003]. The inclusions in this zircon type are mainly apatite and quartz, which would also be compatible with magmatic crystallization. The trace element composition of the zircon cores from sample 2819 is characterized by a strong enrichment in HREE, and pronounced negative Eu anomaly and positive Ce anomaly. These features are also characteristic of igneous zircon [e.g., *Hoskin and Schaltegger*, 2003]. In particular, the negative Eu anomaly indicates that the zircon crystallized in equilibrium with feldspar that strongly partitioned Eu. These zoning and chemical features strongly support a magmatic origin for the 85 Ma zircon in samples 2819 and 1008.

[27] The circa 55 Ma age is recorded in zircon crystals that have similar features to the 85 Ma magmatic zircon. The zoning is sector to oscillatory, Th/U is within magmatic values, and the trace element composition, including the negative Eu anomaly, suggests that the zircon crystallized from a melt. We conclude that the age corresponds to the magmatic crystallization of zircon in samples 3007 and 2912 at 55.6 ± 0.6 and 55.3 ± 0.7 Ma, respectively. If the protolith of sample 2912 was a sedimentary or volcaniclastic rock as is expected, the age of the zircon date the crystallization of the zircon source shortly before deposition of the rock.

[28] Zircon yielding 44 Ma age is substantially different from the magmatic domains. This age is contained in irregular zircon rims that clearly cross cut the oscillatory zoning of the cores. The rims have weakly banded zoning or chaotic patches, more commonly found in metamorphic than magmatic zircon [e.g., *Rubatto and Gebauer*, 2000; *Corfu et al.*, 2003; *Hoskin and Schaltegger*, 2003]. Some of the inclusions contained in the rims of the three samples are diagnostic of high-P metamorphism (phengite, paragonite, barroisitic hornblende) and in most cases are identical to the high-P mineral assemblage of the rocks (Table 1). In particular, phengite inclusions and high-P groundmass phengite in samples 1008 and 2819 are very similar in composition. The trace element composition of the zircon rims (samples 2819 and 3007) are characterized by lower

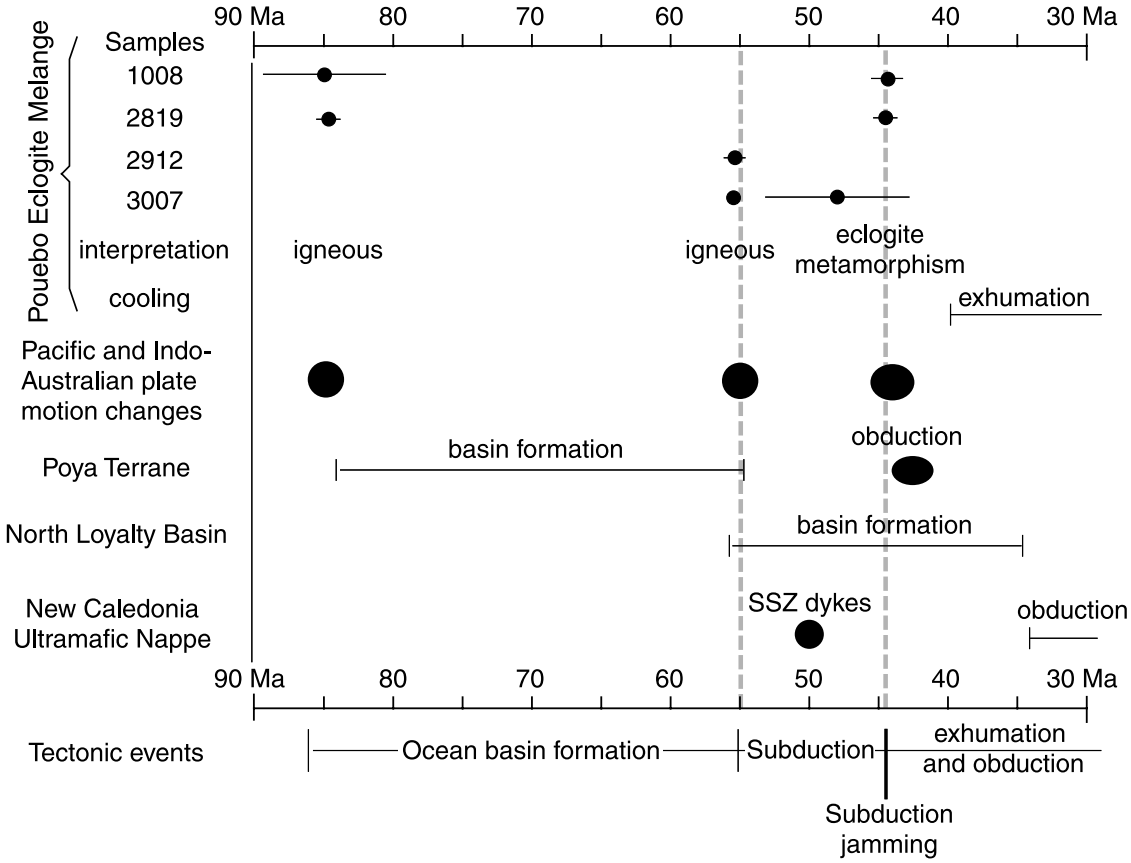

Figure 6. Chronology of eclogite facies samples examined in this study compared with the age of regional geological units and tectonic events. Cooling ages for the Pouébo Eclogite Melange are from *Ghent et al.* [1994] and *Baldwin et al.* [1999]. Changes in plate motion events are from *Yan and Kroenke* [1993], *Hall* [2002], *Crawford et al.* [2003], and *Sdrolias et al.* [2003]. The timing of formation and obduction of the Poya Terrane is from *Cluzel et al.* [2001] and *Ali and Aitchison* [2002], respectively. The age of the North Loyalty Basin is from *Andrews et al.* [1975] and *Sdrolias et al.* [2003]. The timing of dike intrusion and obduction of the New Caledonia ophiolite nappe is from *Cluzel et al.* [2001].

REE contents and much lower Th/U than in the cores. These features have been recognized in zircon formed at relatively low temperature under subsolidus conditions [*Rubatto*, 2002; *Hoskin and Schaltegger*, 2003]. In both samples, the Eu anomaly is close to unity, implying that feldspars were not present at the time of zircon formation [*Rubatto*, 2002]. This feature indicates formation under eclogite facies conditions, as plagioclase is reported to be present in prograde blueschist facies and retrograde greenschist facies mineral assemblages of mafic and metasedimentary rocks of the high-P belt [*Yokoyama et al.*, 1986; *Marmo et al.*, 2002]. The zoning, chemical and inclusion data demonstrate that the circa 44 Ma zircon formed during high-P metamorphism of the samples. The best-constrained ages of this metamorphic stage are 44.1 ± 0.9 Ma and 44.5 ± 1.2 Ma obtained from the pelitic schists 2819 and 1008, respectively.

7. Discussion

7.1. Nature and Timing of Protolith Formation

[29] All of the samples examined in this study have recrystallized under high-P conditions, which prevent protolith identification based on petrography. Fortunately, bulk rock geochemistry and field relationship may be used to constrain the precursor lithologies of the samples. There is little doubt that samples 1008 and 2819 represent metamorphosed pelitic sedimentary rocks. They both derive from sequences with strong compositional layering. Additionally, the composition of both samples directly compares to average shale compositions (Figure 3) and to sedimentary-derived blueschists found in the Diahot Blueschist belt [*Spandler et al.*, 2003].

[30] Geochronological studies of Late Cretaceous rift/drift sedimentary rocks of New Caledonia have revealed that they contain detrital zircon grains ranging from Late Cretaceous (>90 Ma) to Precambrian (~1000 Ma) in age [*Aronson and Tilton*, 1971; *Aitchison et al.*, 1998]. These sedimentary rocks are potential protoliths for pelitic samples 2819 and 1008. However, the zircon cores from samples 2819 and 1008 have uniform ages of 85 Ma, which is inconsistent with derivation from the same continental source regions as the unmetamorphosed rift/drift sedimentary rocks. Instead, the uniform age of the zircon cores of 2819 and 1008 indicates that the original source of these

sedimentary rocks must have been highly restricted and localized, and sedimentation probably occurred soon after formation of the igneous rocks. Possible sources of the zircon cores include rift volcanism related to the opening of a marginal basin or arc magmatism associated with subduction along the Norfolk Ridge. We favor the first hypothesis, as there is little evidence for Late Cretaceous arc magmatism along the Norfolk Ridge or in New Caledonia [*Crawford et al.*, 2003].

[31] Using bulk rock chemistry and mineral inclusions in altered zircon cores, we have previously demonstrated that the protolith of sample 3007 is a seafloor-altered, plagioclase-rich mafic cumulate [*Spandler et al.*, 2004b]. Plagioclase-rich cumulates are a common intrusive rock type of oceanic crust [*Poli and Schmidt*, 2002] which supports the proposal that the eclogite facies rocks from New Caledonia represent previously subducted oceanic crust [*Aitchison et al.*, 1995; *Spandler et al.*, 2004a]. The ~55 Ma igneous zircon cores in 3007 therefore directly relate to a period of oceanic crust formation.

[32] The origin of sample 2912, which also contains magmatic zircon with ~55 Ma age, is more enigmatic. The geochemistry of 2912 is significantly different from samples 1008 and 2819 and may be representative of a felsic igneous rock. However, the relatively small Eu anomaly (Figure 3) and the banded nature of the outcrop are inconsistent with an igneous origin. We suggest that the sample was a sedimentary rock that either had a volcaniclastic origin or represents a quartz-rich facies variant of samples 1008 and 2819. The fact that there is only one age group of detrital magmatic zircon in sample 2912 also indicates a restricted source for this sedimentary rock, such as localized magmatism related to rifting or subduction. Again, we favor a rift origin for the source rocks of this sediment based on the age correlation with zircon from sample 3007.

7.2. Comparison to Unmetamorphosed Rocks of the Poya Terrane

[33] Previous work has shown that the mafic rocks of the PEM have the same chemical characteristics as the nearby Poya Terrane [*Cluzel et al.*, 2001; *Spandler et al.*, 2004a]. Our U-Pb ages for the protolith rocks of the PEM also correlate with paleontological age constraints for the Poya Terrane [*Aitchison et al.*, 1995; *Cluzel et al.*, 2001], further supporting a direct link between the two terranes. *Cluzel et al.* [2001] and *Crawford et al.* [2003] also directly correlated the Poya Terrane with the South Loyalty Basin. Therefore the Poya Terrane, the South Loyalty Basin, and the PEM are interpreted to have been a part of a sediment covered back-arc basin that formed to the north of New Caledonia [*Ali and Aitchison*, 2002] from at least 85 Ma to 55 Ma. We will subsequently refer to this basin as the South Loyalty Basin. Curiously, this age range is almost identical to the period of opening of the Tasman Sea [*Gaina et al.*, 1998] and overlaps with the timing of formation of the Coral Sea [*Yan and Kroenke*, 1993; *Gaina et al.*, 1999], indicating that several independent ocean basins were forming synchronously in the southwest Pacific during the Late Cretaceous to the Eocene.

7.3. Constraints for the Formation of the High-P Rocks

[34] The age of the metamorphic zircon rims on samples 2819, 1008, and 3007 constrain the timing of peak eclogite facies metamorphism to 44 Ma. This represents the first precise constraint for the timing of peak metamorphism, which sheds new light on the formation of the high-P belt of northern New Caledonia. The timing of obduction of the New Caledonia Ultramafic Nappe has recently been redefined to around 34 Ma based on stratigraphic and paleontological constraints [*Cluzel et al.*, 2001]. This is approximately 10 m.y. after the high-P metamorphic event. Hence our age data confirm that high-P metamorphism was unrelated to the overthrusting of the New Caledonia Ultramafic Nappe. Instead, we support the suggestions of *Aitchison et al.* [1995] and *Cluzel et al.* [2001] that high-P metamorphism resulted from subduction of oceanic crust and associated sedimentary rocks. The preservation of contemporaneous SSZ dikes and boninites associated with the forearc-derived New Caledonia Ultramafic Nappe [*Eissen et al.*, 1998; *Cluzel et al.*, 2001] further supports a subduction origin for the high-P rocks.

[35] Samples 2912 and 3007 provide evidence that oceanic crust and sediments formed at ~55 Ma. Hence there is only a maximum of 11 m.y. between the final stage of magmatic formation of the oceanic crust and subduction to depths of approximately 60 km. This implies a minimum burial rate of 0.55 cm/yr. Additionally, these data suggest that subduction is not likely to be very advanced. Although there is no data at this time in the area of consideration, assuming convergence rates of 3–5 cm/yr results in a maximum of 330–550 km of oceanic crust being subducted. This limited length of the slab combined with the short time of subduction suggests that the thermal condition within the slab probably did not reach steady state conditions. Geophysical models of subduction zones suggest that initial stages of subduction of such young oceanic crust would lead to relatively hot thermal conditions of subduction and possibly slab melting [*Peacock*, 1996; *Kincaid and Sacks*, 1997]. The peak metamorphic conditions of around 1.9 GPa and 600°C [*Carson et al.*, 1999] are situated in the region of the hottest geotherms modeled by *Kincaid and Sacks* [1997] in agreement with the age data presented here. The presence of boninites that formed contemporaneously with subduction within the forearc-derived New Caledonia Ultramafic Nappe further supports this premise, as boninite genesis requires relatively high temperatures in the forearc region of subduction zones [*Crawford et al.*, 1989].

[36] Attempted subduction of the continental margin of the Norfolk Ridge and its sedimentary cover is invoked as a cause of subduction jamming. The 44 Ma age of high-P metamorphism of the PEM represent the timing of attempted subduction of continental sediments and hence is interpreted to closely comply with the timing of this subduction jamming (Figure 6). Available K-Ar and ^{40}Ar-^{39}Ar ages on phengite and K-feldspar yield ages of 40–34 Ma [*Ghent et al.*, 1994; *Baldwin et al.*, 1999]. These

ages are interpreted to represent cooling after a high-P greenschist facies metamorphic event, which occurred at depths of about 30 km (P $\sim$ 0.9 GPa, T $\sim$ 510°C [*Marmo et al.*, 2002]). Hence the PEM must have experienced significant exhumation shortly after reaching peak metamorphic conditions at 44 Ma. Our data fits very well the structural evolution of the high-P belt proposed by *Rawling and Lister* [1999, 2002]. They proposed that convergence and related high-P metamorphism was followed by a period of extension leading to exhumation of the PEM. Such extensional tectonic might have also affected the adjacent oceanic crust and could have caused denudation of the former forearc mantle wedge (Figure 7d). Renewed convergence is documented in the obduction of these mantle rocks over the sediments and continental basement, forming the New Caledonia Ultramafic Nappe. We suggest that this convergence caused the intense upright folding and the related large-scale antiform, in which the high-P rocks are found today [*Clarke et al.*, 1997; *Rawling and Lister*, 1999] (Figure 1). Nonetheless, obduction of the New Caledonia Ultramafic Nappe is not expected to have caused significant increase in T in the high-P belt, as there is no evidence of resetting of isotopic systems at this time (34 Ma) [*Ghent et al.*, 1994; *Baldwin et al.*, 1999].

7.4. Tectonic Implications

[37] A key component to all previous plate tectonic models for the southwest Pacific is the timing of ocean floor formation and subduction in the New Caledonia region, yet the chronology of these events have been poorly constrained prior to this study. By incorporating our U-Pb dating results with previously published geological data and models (Figure 6), we are able to better constrain the tectonic evolution of the New Caledonia region from the Late Cretaceous to the end of the Eocene.

[38] The onset of Gondwana breakup at the end of the Cretaceous led to the synchronous opening of the Tasman Sea and the South Loyalty Basin between 85 Ma and 52 Ma, causing rifting of the Lord Howe Rise and Norfolk Ridge away from the Gondwana margin. During this period sediments derived from the Norfolk Ridge and contemporaneous volcanic activity were deposited in the newly forming South Loyalty Basin adjacent to the northern margin of the Norfolk Ridge. *Cluzel et al.* [2001] and *Crawford et al.* [2003] suggest that southwest dipping subduction of the Pacific Ocean crust led to formation of the back-arc South Loyalty Basin immediately to the north of the Norfolk Ridge. Although there is no known arc of this age preserved in the region, *Crawford et al.* [2003] suggest that arc volcanism may have been suppressed by rapid slab rollback and back-arc extension. Alternatively, northeast dipping subduction immediately southwest of the Norfolk Ridge may also have initiated back-arc spreading in the South Loyalty Basin [*Collot et al.*, 1987]. However, there is little evidence of a magmatic arc development on New Caledonia or Norfolk Ridge at this time. Further work is required to resolve these issues.

[39] At around 55 Ma, there were major changes in the motions of the Pacific and Australian plates [*Yan and Kroenke*, 1993; *Crawford et al.*, 2003], possibly caused by the initial collision of India with Asia [*Rowley*, 1996]. Seafloor spreading ceased in the Tasman Sea, Coral Sea, and the South Loyalty Basin [*Gaina et al.*, 1998; *Crawford et al.*, 2003]. We support the proposal of *Cluzel et al.* [2001] and *Crawford et al.* [2003] that northward dipping subduction was initiated within the South Loyalty Basin at this time (Figure 7a). Although our data provides evidence that this was only a short-lived subduction system, the generally high temperature of subduction might have favored the production of a small arc (Loyalty Arc; Figure 7b). Evidence of arc magmatism during this subduction event is preserved as boninitic rocks and SSZ mafic dikes within the forearc-derived New Caledonia Ultramafic Nappe [*Eissen et al.*, 1998; *Cluzel et al.*, 2001]. The lateral extent of this arc is unknown, but may have been continuous with contemporaneous subduction occurring in the New Guinea region [*Weiland et al.*, 1997; *Hall*, 2002]. The convergence progressively consumed the South Loyalty Basin, causing the migration of New Caledonia and the Norfolk Ridge toward the trench. The initiation of subduction may have also been coupled with contemporaneous formation of the North Loyalty Basin as a back-arc basin to the Loyalty Arc (Figure 6).

[40] Subduction continued to consume the South Loyalty Basin until 44 Ma, when the sedimentary pile flanking the northern side of the Norfolk Ridge entered the trench and jammed the subduction zone (Figure 7c). Partial subduction of the sediments to depths of up to 50 km caused relatively high-P, low-T metamorphism and formation of the Diahot Blueschists. Some sedimentary material was subducted to greater depths ($\sim$60 km) to form part of the PEM. Jamming of the subduction zone probably resulted in the obduction of some slices of oceanic crust and sediments that now comprise the Poya Terrane and adjacent Late Cretaceous-Eocene sedimentary rocks (Figure 7c). The timing of emplacement of the Poya Terrane is poorly constrained, but is expected to be around 43 Ma [*Eissen et al.*, 1998; *Ali and Aitchison*, 2002], simultaneously or slightly after peak high-P metamorphism occurred in the PEM.

[41] In the New Caledonia region, a short period of extension led to the exhumation of the Diahot Blueschist and PEM at 40–35 Ma to midcrustal levels (Figure 7d) [*Baldwin et al.*, 1999]. The rapid exhumation may have been driven by buoyancy after slab break-off [*Cluzel et al.*, 2001] or may be related to extension associated with the

Figure 7. Tectonic model for the New Caledonia region from the Paleocene to late Eocene. Note that the diagrams are not drawn to scale. The model depicts subduction initiation, formation of the Loyalty Arc, subduction jamming, exhumation of the high-P rocks, and obduction of the Poya Terrane and New Caledonia Ultramafic Nappe. SLB, South Loyalty Basin; NCUN, New Caledonia Ultramafic Nappe; DB, Diahot Blueschists; PEM, Pouébo Eclogite Melange; PT, Poya Terrane.

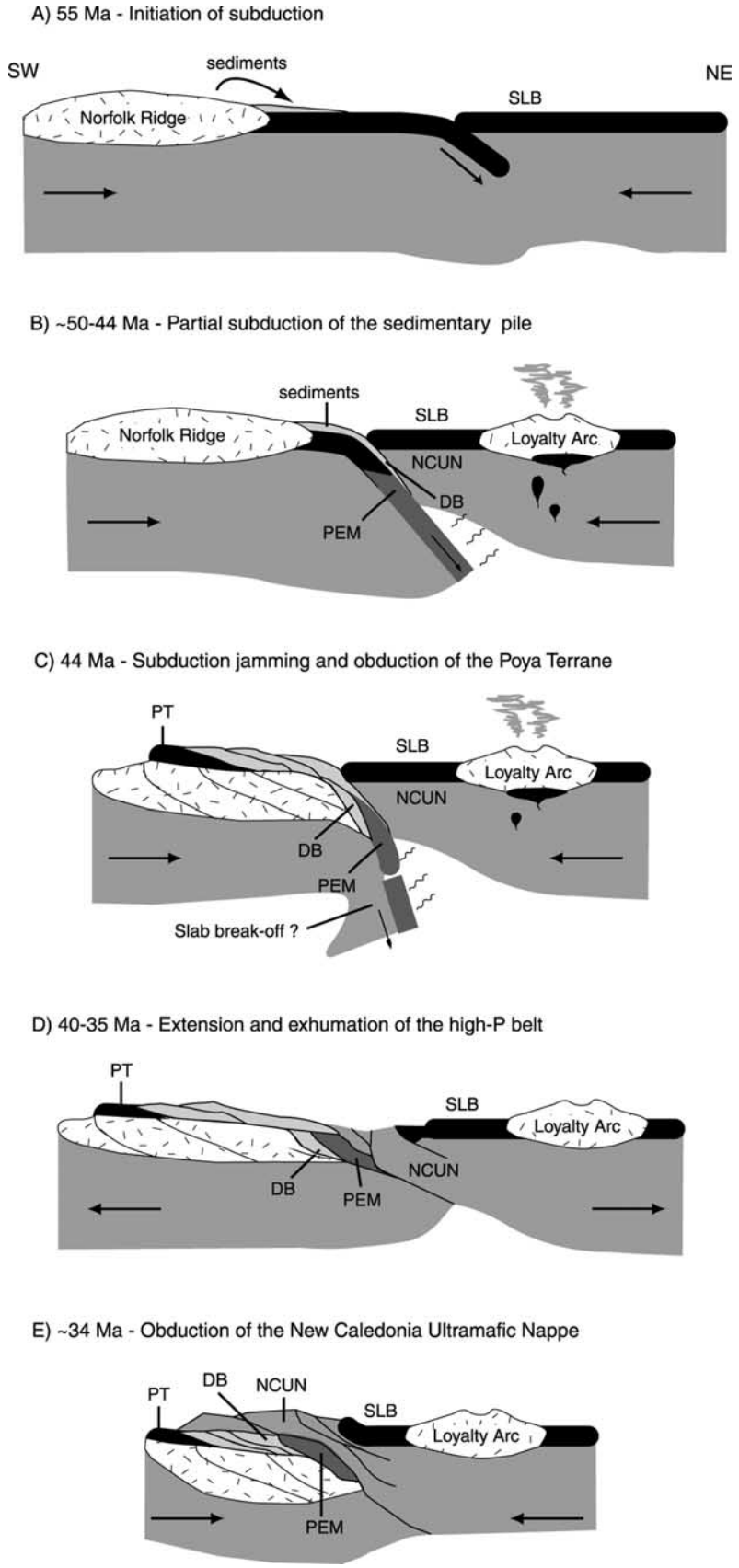
A) 55 Ma - Initiation of subduction
SW
sediments
NE
SLB
Norfolk Ridge
B) ~50-44 Ma - Partial subduction of the sedimentary pile
sediments
SLB
Norfolk Ridge
Loyalty Arc
NCUN
DB
PEM
C) 44 Ma - Subduction jamming and obduction of the Poya Terrane
PT
SLB
Loyalty Arc
NCUN
DB
PEM
Slab break-off ?
D) 40-35 Ma - Extension and exhumation of the high-P belt
PT
SLB
Loyalty Arc
NCUN
DB
PEM
E) ~34 Ma - Obduction of the New Caledonia Ultramafic Nappe
PT
DB
NCUN
SLB
Loyalty Arc
PEM

Figure 7

roll-back of a subducting slab to the southwest of the Norfolk Ridge [*Rawling and Lister*, 1999], or a combination of these processes.

[42] Renewed compression in the region caused the obduction of the Loyalty forearc lithosphere over New Caledonia at 34 Ma (Figure 7e) [*Auzende et al.*, 2000; *Cluzel et al.*, 2001] and the initiation of a new west dipping subduction system to the northeast of the North Loyalty Basin [*Hall*, 2002; *Crawford et al.*, 2003]. The North Loyalty Basin may have been in a back-arc setting to the new subduction system, allowing continuation of magmatism in the basin until 35 Ma [*Sdrolias et al.*, 2003].

[43] The above tectonic model is very similar to the models proposed by *Eissen et al.* [1998], *Cluzel et al.* [2001], and *Crawford et al.* [2003]. However, these previous models have assumed that the high-P metamorphism and subduction jamming in New Caledonia occurred during the late Eocene (40–34 Ma) and was temporally associated with the obduction of the New Caledonia Ultramafic Nappe. A significant new constraint in our model is the dating of high-P metamorphism and subduction jamming in northern New Caledonia to 44 Ma. Our data, combined with previous work, indicates that there was at least a 10 m.y. time span between subduction jamming at 44 Ma to the final forearc ophiolite obduction at 34 Ma. New Caledonia is likely to have undergone several compressional and extensional episodes during this period [e.g., *Rawling and Lister*, 2002].

7.5. Implications for Regional Plate Tectonics at ~44 Ma

[44] Between 45 and 43 Ma, there was a significant change in the plate motions of the Pacific and Indo-Australian Plates [*Yan and Kroenke*, 1993; *Crawford et al.*, 2003] and a major plate reorganization in the southeast Asia region [*Hall*, 2002]. The most recognized manifestation of these changes is the bend in the Hawaii-Emperor seamount chain in the Pacific. However, other significant events in the region include compressional deformation in Queensland and the Lord Howe Rise [*Symonds et al.*, 1999; *Veevers*, 2000], the fusion of the Australian and Indian Plates [*Veevers*, 2000; *Hall*, 2002], and the initiation of new subduction systems throughout the western Pacific, including the Tonga-Kermadec arc [*Clift and MacLeod*, 1999], the Melanesian arc in Vanuatu [*Crawford et al.*, 2003], the Solomon Islands [*Petterson et al.*, 1999], New Britain and New Ireland (*Hall*, 2002), the Palau-Kyushu Ridge arc [*Deschamps and Lallemand*, 2002], and the North Sulawesi arc [*Polvé et al.*, 1997]. The rapid increase in velocity of the Australian and Pacific Plates at this time [*Veevers*, 2000] may have caused an increase in the rate of arc volcanism, which produced relatively high atmospheric CO_2 levels and middle Eocene global warming [*Bohaty and Zachos*, 2003].

[45] It is clear that the 45–43 Ma plate reorganization had a major effect on crustal growth, global climate, and present-day plate tectonic configurations. However, it is unclear what the causes of these events were. Major collisions and suturing of plates in the New Guinea, Indonesia, and Philippines regions did not take place until post Eocene times [*Pigram and Davies*, 1987; *Hall*, 1996; *Deschamps and Lallemand*, 2002; *Yumul et al.*, 2003]. *Hall* [1996] suggests that instigation may have come from collision between India and Asia, but as shown by *Rowley* [1996], this collision was almost certainly diachronous and began at least 10 m.y. earlier. Therefore we speculate that the newly constrained 44 Ma collision of New Caledonia and northern Norfolk Ridge with the Loyalty subduction zone may be partially responsible for contemporaneous plate reorganization in the southwest Pacific.

8. Conclusions

[46] Using U-Pb SHRIMP dating, we present new constraints on the age of the protoliths and timing of high-P metamorphism for the eclogite facies rocks of northern New Caledonia. Magmatic zircon cores from three pelitic/felsic samples and one mafic sample provided consistent ages of circa 85 and 55 Ma, while zircon rims that overgrew the magmatic cores during high-P metamorphism were dated at 44 Ma. The age of the magmatic zircon further support a direct relationship between the eclogite facies rocks and the mafic Poya Terrane of western New Caledonia, and indicates that a major ocean basin was forming to the north of New Caledonia during the Late Cretaceous to Eocene. The newly constrained mid-Eocene age for high-P metamorphism indicates that subduction preceded overthrusting of the New Caledonia Ultramafic Nappe by circa 10 m.y. It is expected that the age of high-P metamorphism also closely dates the timing of subduction jamming due to attempted subduction of the Norfolk Ridge. This event is likely to have affected the contemporaneous tectonic reconfiguration of the region, which include major changes in motions of the Australian and Pacific Plates and the initiation of several new subduction systems.

[47] **Acknowledgments.** This work was supported by the Australian Research Council and the ANU. We thank Gordon Lister for fruitful discussions on New Caledonian geology and comments on an early version of the manuscript. The paper also benefited from insightful reviews by Ian Buick and an anonymous reviewer.

References

Aitchison, J., G. L. Clarke, S. Meffre, and D. Cluzel (1995), Eocene arc-continent collision in New Caledonia and implications for regional southwest Pacific tectonic evolution, *Geology*, *23*, 161–164.

Aitchison, J., T. R. Ireland, G. L. Clarke, D. Cluzel, A. M. Davis, and S. Meffre (1998), Regional implications of U/Pb SHRIMP age constraints on the tectonic evolution of New Caledonia, *Tectonophysics*, *299*, 333–343.

Ali, J. R., and J. C. Aitchison (2002), Palaeomagnetic-tectonic study of the New Caledonia Koh Ophiolite and the mid-Eocene obduction of the Poya Terrane, *N. Z. J. Geol. Geophys.*, *45*, 313–322.

Andrews, J. E., et al. (1975), Site 286, *Initial Rep. Deep Sea Drill. Proj.*, *30*, 69–91.

Aronson, J. L., and G. R. Tilton (1971), Probable Precambrian detrital zircons in New Caledonia and southwest Pacific continental structure, *Geol. Soc. Am. Bull.*, *82*, 3449–3456.

Auzende, J.-M., S. Van de Beuque, M. Régnier, Y. Lafoy, and P. Symonds (2000), Origin of the New Caledonian ophiolites based on a French-Australian seismic transect, *Mar. Geol.*, *162*, 225–236.

Baldwin, S. L., T. Rawling, and P. G. Fitzgerald (1999), Thermochronology of the northern high P/T terrane of New Caledonia: Implications for mid-Tertiary plate boundary processes in the SW Pacific, in *Penrose Conference, 1999: Mid-Cretaceous to Recent Plate Boundary Processes in the Southwest Pacific, Abstract Volume*, edited by S. L. Baldwin and G. S. Lister, pp. 13–14, Geol. Soc. of Am., Boulder, Colo.

Black, L. P., S. L. Kamo, C. M. Allen, J. N. Aleinikoff, D. W. Davis, R. J. Korsch, and C. Foudoulis (2003), TEMORA 1: A new zircon standard for Phanerozoic U-Pb geochronology, *Chem. Geol.*, *200*, 155–170.

Bohaty, S. M., and J. C. Zachos (2003), Significant Southern Ocean warming event in the late middle Eocene, *Geology*, *31*, 1017–1020.

Carson, C. J., R. Powell, and G. L. Clarke (1999), Calculated mineral equilibria for eclogites in CaO-Na_2O-FeO-MgO-Al_2O_3-SiO_2-H_2O: Application to the Pouebo Terrane, Pam Peninsula, New Caledonia, *J. Metamorph. Geol.*, *17*, 9–24.

Clarke, G. L., J. C. Aitchison, and D. Cluzel (1997), Eclogites and blueschists of the Pam Peninsula, NE New Caledonia: A reappraisal, *J. Petrol.*, *38*, 843–876.

Clift, P. D., and C. J. MacLeod (1999), Slow rates of subduction erosion estimated from subsidence and tilting of the Tonga forearc, *Geology*, *27*, 411–414.

Cluzel, D., J. C. Aitchison, and C. Picard (2001), Tectonic accretion and underplating of mafic terranes in the late Eocene intraoceanic fore-arc of New Caledonia (southwest Pacific): Geodynamic implications, *Tectonophysics*, *340*, 23–59.

Collot, J. Y., J. Daniel, and R. V. Burne (1985), Recent tectonics associated with the subduction/collision of the D'Entrecasteuax zone in the central New Hebrides, *Tectonophysics*, *112*, 325–356.

Collot, J. Y., A. Malahoff, J. Recy, G. Latham, and F. Missague (1987), Overthrust emplacement of the New Caledonian ophiolite: Geophysical evidence, *Tectonics*, *6*, 215–232.

Compston, W., I. S. Williams, J. L. Kirschvink, Z. Zhang, and G. Ma (1992), Zircon U-Pb ages for the Early Cambrian time-scale, *J. Geol. Soc. London*, *149*, 171–184.

Corfu, F., J. M. Hanchar, P. W. O. Hoskin, and P. Kinny (2003), Atlas of zircon textures, in *Zircon*, *Rev. Mineral.*, vol. 53, edited by J. M. Hanchar and P. W. O. Hoskin, pp. 469–500, Mineral. Soc. of Am., Washington, D. C.

Crawford, A. J., T. J. Falloon, and D. H. Green (1989), Classification, petrogenesis and tectonic setting of boninites, in *Boninites*, edited by A. J. Crawford, pp. 1–49, CRC Press, Boca Raton, Fla.

Crawford, A. J., S. Meffre, and P. A. Symonds (2003), 120 to 0 Ma tectonic evolution of the southwest Pacific and analogous geological evolution of the 600 to 220 Ma Tasman Fold Belt system, *Spec. Pap. Geol. Soc. Am.*, *372*, 383–403.

Deschamps, A., and S. Lallemand (2002), The West Philippine Basin: An Eocene to early Oligocene back arc basin opened between two opposed subduction zones, *J. Geophys. Res.*, *107*(B12), 2322, doi:10.1029/2001JB001706.

Eissen, J. P., A. J. Crawford, J. Cotten, S. Meffre, H. Bellon, and M. Delaune (1998), Geochemistry and tectonic significance of basalts in the Poya Terrane, New Caledonia, *Tectonophysics*, *284*, 203–220.

Fitzherbert, J. A., G. L. Clarke, B. Marmo, and R. Powell (2004), The origin and P-T evolution of peridotites and serpentinites of NE New Caledonia: Prograde interaction between continental margin and the mantle wedge, *J. Metamorph. Geol.*, *22*, 327–344.

Gaina, C., R. D. Müller, J. Y. Royer, J. M. Stock, J. Hardebeck, and P. Symonds (1998), The tectonic history of the Tasman Sea: A puzzle with thirteen pieces, *J. Geophys. Res.*, *103*, 12,413–12,433.

Gaina, C., R. D. Müller, J. Y. Royer, and P. Symonds (1999), Evolution of the Louisiade Triple Junction, *J. Geophys. Res.*, *104*, 12,927–12,939.

Ghent, E. D., J. C. Roddick, and P. M. Black (1994), ^{40}Ar-^{39}Ar dating of white micas from the epidote to the omphacite zones, northern New Caledonia: Tectonic implications, *Can. J. Earth Sci.*, *31*, 995–1001.

Hall, R. (1996), Reconstructing Cenozoic SE Asia, in *Tectonic Evolution of Southeast Asia*, edited by R. Hall and D. Blundell, *Geol. Soc. Spec. Publ.*, *106*, 153–184.

Hall, R. (2002), Cenozoic geological and plate tectonic evolution of SE Asia and the SW Pacific: Computer-based reconstructions, model and animations, *J. Asian Earth Sci.*, *20*, 353–431.

Hoskin, P. W. O., and U. Schaltegger (2003), The composition of zircon and igneous and metamorphic petrogenesis, in *Zircon*, *Rev. Mineral.*, vol. 53, edited by J. M. Hanchar and P. W. O. Hoskin, pp. 27–62, Mineral. Soc. of Am., Washington, D. C.

Hoskin, P. W. O., P. D. Kinny, D. Wyborn, and B. W. Chappell (2000), Identifying accessory mineral saturation during differentiation in granitoid magmas: An integrated approach, *J. Petrol.*, *41*, 1365–1396.

Kincaid, C., and I. S. Sacks (1997), Thermal and dynamical evolution of the upper mantle in subduction zones, *J. Geophys. Res.*, *102*, 12,295–12,315.

Ludwig, K. R. (2000), Isoplot/Ex version 2.4, A geochronological toolkit for Microsoft Excel, special publication, 56 pp., Berkeley Geochron. Cent., Berkeley, Calif.

Marmo, B. A., G. L. Clarke, and R. Powell (2002), Fractionation of bulk rock composition due to porphyroblast growth: Effects on eclogite facies mineral equilibria, Pam Peninsula, New Caledonia, *J. Metamorph. Geol.*, *20*, 151–165.

Maurizot, P., J.-M. Eberle, C. Habault, and C. Tessarollo (1989), Notice explicative Sur La Feuille Pam-Ouegoa, Bur. de Rech. Geol. et Minieres, Noumea, New Caledonia.

Peacock, S. M. (1996), Thermal and petrologic structure of subduction zones, in *Subduction Top to Bottom*, *Geophys. Monogr. Ser.*, vol. 96, edited by G. W. Bebout et al., pp. 119–133, AGU, Washington, D. C.

Pearce, N. J. G., W. T. Perkins, J. A. Westgate, M. J. Gorton, S. E. Jackson, C. R. Neal, and S. P. Chenery (1997), A compilation of new and published major and trace element data for NIST SRM 610 and NIST SRM 612 glass reference materials, *Geostand. Newsl.*, *21*, 115–144.

Petterson, M. G., et al. (1999), Geological-tectonic framework of the Solomon Islands, SW Pacific: Crustal accretion and growth within and intra-oceanic setting, *Tectonophysics*, *301*, 35–60.

Pigram, C. J., and H. L. Davies (1987), Terranes and the accretion history of the New Guinea orogen, *BMR J. Aust. Geol. Geophys.*, *10*, 193–211.

Poli, S., and M. W. Schmidt (2002), Petrology of subducted slabs, *Annu. Rev. Earth Planet. Sci.*, *30*, 207–235.

Polvé, M., R. C. Maury, H. Bellon, C. Rangin, B. Priadi, S. Yuwono, J. L. Joron, and R. Soeria Atmadja (1997), Magmatic evolution of Sulawesi (Indonesia): Constraints on the Cenozoic geodynamic history of the Sundaland active margin, *Tectonophysics*, *272*, 69–92.

Rawling, T. J., and G. S. Lister (1999), Oscillating modes of orogeny in the southwest Pacific and the tectonic evolution of New Caledonia, in *Exhumation Processes: Normal Faulting, Ductile Flow and Erosion*, edited by U. Ring et al., *Geol. Soc. Spec. Publ.*, *154*, 109–127.

Rawling, T. J., and G. S. Lister (2002), Large-scale structure of the eclogite-blueschist belt of New Caledonia, *J. Struct. Geol.*, *24*, 1239–1258.

Rowley, D. B. (1996), Age of initiation of collision between India and Asia: A review of stratigraphic data, *Earth Planet. Sci. Lett.*, *145*, 1–13.

Rubatto, D. (2002), Zircon trace element geochemistry; partitioning with garnet and the link between U-Pb ages and metamorphism, *Chem. Geol.*, *184*, 123–138.

Rubatto, D., and D. Gebauer (2000), Use of cathodoluminescence for U-Pb zircon dating by ion microprobe: Some examples from the western Alps, in *Cathodoluminescence in Geosciences*, edited by M. Pagel et al., pp. 373–400, Springer, New York.

Sdrolias, M., R. D. Müller, and C. Gaina (2003), Tectonic evolution of the southwest Pacific using constraints from backarc basins, *Spec. Pap. Geol. Soc. Am.*, *372*, 343–359.

Spandler, C. J., J. Hermann, R. J. Arculus, and J. A. Mavrogenes (2003), Redistribution of trace elements during prograde metamorphism from lawsonite blueschist to eclogite facies; implications for deep subduction-zone processes, *Contrib. Mineral. Petrol.*, *146*, 205–222.

Spandler, C. J., J. Hermann, R. J. Arculus, and J. A. Mavrogenes (2004a), Geochemical heterogeneity and element mobility in deeply subducted oceanic crust; insights from high-pressure mafic rocks from New Caledonia, *Chem. Geol.*, *206*, 21–42.

Spandler, C. J., J. Hermann, and D. Rubatto (2004b), Exsolution of thortveitite, yttrialite and xenotime during low temperature recrystallization of zircon from New Caledonia, and their significance for trace element incorporation in zircon, *Am. Mineral.*, *89, 1795–1806.*

Symonds, P., H. Stagg, and I. Borissova (1999), The transition from rifting and break-up to convergence in the Lord Howe Rise–Norfolk Ridge region, in *Penrose Conference, 1999: Mid-Cretaceous to Recent Plate Boundary Processes in the Southwest Pacific, Abstract Volume*, edited by S. L. Baldwin and G. S. Lister, pp. 94–95, Geol. Soc. of Am., Boulder, Colo.

Taylor, S. R., and S. M. McLennan (1985), *The Ccontinental Crust: Its Composition and Evolution*, 312 pp., Blackwell, Malden, Mass.

Tomaschek, F., A. K. Kennedy, I. M. Villa, M. Lagos, and C. Ballhaus (2003), Zircons from Syros, Cyclades, Greece: Recrystallization and mobilization of zircon during high-pressure metamorphism, *J. Petrol.*, *44*, 1977–2002.

Veevers, J. J. (2000), Change of tectono-stratigraphic regime in the Australian plate during the 99 Ma (mid-Cretaceous) and 43 Ma (mid-Eocene) swerves of the Pacific, *Geology*, *28*, 47–50.

Weiland, R. J., F. W. McDowell, W. Sunyoto, B. Sapie, and M. Cloos (1997), K-Ar whole rock ages from the Yeleme blueschist of western New Guinea, *Geol. Soc. Am. Abstr. Programs*, *29*, 230.

Williams, I. (1998), U-Th-Pb geochronology by ion microprobe, in *Application of Microanalytical Techniques to Understanding Mineralizing Processes*, Reviews in Economic Geology, vol. 7, edited by M. A. McKibben, W. C. Shanks III, and W. I. Ridley, pp. 1–35, Soc. of Econ. Geol., Inc., Littleton, Colo.

Yan, C. Y., and L. W. Kroenke (1993), A plate tectonic reconstruction of the southwest Pacific, 0–100 Ma, *Proc. Ocean Drill. Program, Sci. Results*, *130*, 697–707.

Yokoyama, K., R. N. Brothers, and P. M. Black (1986), Regional eclogite facies in the high-pressure metamorphic belt of New Caledonia, in *Blueschists and Eclogites*, edited by B. W. Evans, and E. H. Brown, *Mem. Geol. Soc. Am.*, *164*, 407–423.

Yumul, G. P.Jr., C. B. Diamalanta, R. A. Tamayo Jr., and R. C. Maury (2003), Collision, subduction and accretion events in the Philippines: A synthesis, *Island Arc*, *12*, 77–91.

J. Hermann, Research School of Earth Sciences, Australian National University, Canberra ACT 0200, Australia.

D. Rubatto and C. Spandler, Department of Earth and Marine Sciences, Australian National University, Canberra ACT 0200, Australia. (carl@ems.anu.edu.au)